ISSN 1990-7931, Russian Journal of Physical Chemistry B, 2025, Vol. 19, No. 1, pp. 236–254. © Pleiades Publishing, Ltd., 2025.

CHEMICAL PHYSICS OF NANOMATERIALS

Doping Effects in Ternary Aluminum Gallium Nitride Hetero-Cluster Towards High-Electron-Mobility Transistors for Hydrogen Sensing: A Density Functional Theory Study and Energy-Saving

F. Mollaamin[a, *] and M. Monajjemi[b]

[a] *Department of Biomedical Engineering, Faculty of Engineering and Architecture, Kastamonu University, Kastamonu, Turkey*

[b] *Department of Chemical Engineering, Central Tehran Branch, Islamic Azad University, Tehran, Iran*

**e-mail: fmollaamin@kastamonu.edu.tr*

Received September 2, 2024; revised September 15, 2024; accepted September 20, 2024

Abstract—The nitrogen-polar AlGaN structure is expected to have higher carrier density when it is doped with semiconductor atoms of silicon (Si) or germanium (Ge) and noble metals of palladium (Pd) or platinum (Pt). So, the metal-polar AlGaN electronic devices offer various advantages, such as high breakdown voltage and high-temperature operation. A comprehensive investigation on hydrogen grabbing towards formation of hetero-clusters of AlGaN–H, Si–AlGaN–H, Ge–AlGaN–H, Pd–AlGaN–H, Pt–AlGaN–H was carried out using DFT computations at the CAM–B3LYP–D3/6-311+G(d, p) level of theory. The notable fragile signal intensity close to the parallel edge of the nanocluster sample might be owing to silicon or germanium binding induced non-spherical distribution of Si–AlGaN or Ge–AlGaN hetero-clusters. However, a considerable deviation exists from doping atoms of palladium or platinum as electron acceptors on the surface of Pd–AlGaN or Pt–AlGaN hetero-clusters. The doped Si, Ge, Pd, Pt atoms with their nearby N4, N7, N12 atoms in hybrid materials of Si–AlGaN, Ge–AlGaN, Pd–AlGaN, Pt–AlGaN, then N atoms are spin polarized and couple with Si, Ge, Pd, Pt atoms, which result in magnetism. Based on TDOS, the excessive growth technique on doping silicon, germanium, palladium or platinum is a potential approach to designing high efficiency hybrid semipolar gallium nitride devices in a long wavelength zone. The advantages of platinum or palladium over aluminum gallium nitride include its higher electron and hole mobility, allowing platinum or palladium doping devices to operate at higher frequencies than silicon or germanium doping devices. In fact, the study of Si-/Ge-/Pd-/Pt-doped AlGaN hetero-cluster shows promise for a high-performance electronic device and hydrogen gas sensing applications.

Keywords: aluminum gallium nitride, transistor, energy storage, silicon, germanium, palladium, platinum

DOI: 10.1134/S1990793124701689

1. INTRODUCTION

A binary III/V direct bandgap semiconductor called Gallium nitride (GaN) is a very hard material with wide bandgap applied in a variety of technologies, including optoelectronic, high-power electronics and light-emitting diodes, partly due to its favorable thermal properties [1, 2]. The nitrides of group III in periodic table have low sensitivity to ionizing radiation which make them appropriate materials for solar cell arrays for satellites. Therefore, space applications could also benefit as devices have shown stability in high radiation environments. Ternary AlGaN alloys have been recognized as promising materials for realizing deep ultraviolet (DUV) optoelectronic devices with operating wavelengths down to 200 nm [1–3]. For the development of high performance AlGaN-based DUV devices, high-conductivity *p*-type Al-rich $Al_xGa_{1-x}N$ ($x \geq 0.4$) is essential. Many studies have shown that enhancing the *p*-type conductivity has a significant effect on the improvement of both the electrical and optical properties of AlGaN DUV optoelectronics [4–8].

The influence of two different methods of silicon doping in AlGaN layer, that is, modulation-doping (MD) and delta-doping (DD), on the optical and electrical performance of deep ultraviolet light-emitting diodes (DUV-LEDs) has been investigated. Both the photoluminescence and electroluminescence intensities in the Si-DD structure are stronger than those obtained by the Si-MD method, while the forward voltage and reverse leakage current are slightly smaller in the DD structure than that in the MD structure. Compared with the MD structure, the DD structure shows higher capacitance-voltage characteristics. This study suggests that the DD method can improve the optical and electrical performance of DUV-LEDs [9].

The researchers have reported the effect of germanium as *n*-type dopant on the electrical and optical properties of $Al_xGa_{1-x}N$ layers grown by plasma-assisted molecular-beam epitaxy. The Al content has been varied from $x=0$ to 0.66, confirmed by Rutherford backscattering spectrometry, and the Ge concentration was increased up to $[Ge]=1\times10^{21}$ cm^{-3}. Even at these high doping levels (>1% atomic fraction) Ge does not induce any structural degradation in $Al_xGa_{1-x}N$ layers with $x<0.15$. However, for higher Al compositions, clustering of Ge forming crystallites was observed. Hall effect measurements show a gradual decrease of the carrier concentration when increasing the Al mole fraction, which is already noticeable in samples with $x = 0.24$. Samples with $x = 0.64$–0.66 remain conductive ($\sigma = 0.8$–$0.3\ \Omega^{-1}$ cm^{-1}), but the donor activation rate drops to around 0.1% (carrier concentration around 1×10^{18} cm^{-3} for $[Ge]\approx1\times10^{21}$ cm^{-3}). From the optical point of view, the low temperature photoluminescence is dominated by the band-to-band emission, which shows only the spectral shift and broadening associated to the Burstein–Moss effect. The evolution of the photoluminescence peak position with temperature shows that the free carriers due to Ge doping can efficiently screen the potential fluctuations induced by alloy disorder [10].

Energy-saving photodetectors are the key components in future photonic systems. Particularly, self-powered photoelectrochemical-type photodetectors (PEC–PDs), which depart completely from the classical solid-state junction device, have lately intrigued intensive interest to meet next-generation power-independent and environment-sensitive photodetection. Herein, we construct, for the first time, solar-blind PEC PDs based on self-assembled AlGaN nanostructures on silicon. Importantly, with the proper surface platinum (Pt) decoration, a significant boost of photon responsivity by more than an order of magnitude was achieved in the newly built Pt/AlGaN nanoarchitectures, demonstrating strikingly high responsivity of 45 mA/W and record fast response/recovery time of 47/20 ms without external power source. Such high solar-blind photodetection originates from the unparalleled material quality, fast interfacial kinetics, as well as high carrier separation efficiency which suggests that embracement of defect-free wide-bandgap semiconductor nanostructures with appropriate surface decoration offers an unprecedented opportunity for designing future energy-efficient and large-scale optoelectronic systems on a silicon platform [11, 12].

Moreover, it was demonstrated that a Pd gated high electron mobility transistor (HEMT) based on the AlGaN/GaN multilayers structure. A critical Pd thickness as small as 2 nm was utilized to shorten the H atoms diffusion distance so that its performances in low concentrations could be improved [13–19]. Recently, the researchers have calculated using DFT method [20–28] the alloy-disorder-limited electron mobility of $Al_xGa_{1-x}N$ from first principles as a technologically important ultra-wide-bandgap alloy with promise in light emitting diodes and high-power transistors [29–32].

In our previous works, the investigation of energy storage in fuel cells through hydrogen adsorption has been accomplished using DFT calculations through different nanomaterials consisting of silicon/germanium/tin/lead nano-carbides [33], magnesium -aluminum alloy [34] and aluminum/carbon/silicon doping boron nitride nanocage [35]. Nanomaterials with remarkable specific structures indicate promising applications in the field of energy storage, electrocatalysis, and fuel cells [36–43]. In this paper, we propose a feasible ternary semiconductor of aluminum gallium nitride which is doped with silicon, germanium, palladium or platinum. We carried out molecular modelling considering the geometrical parameters of doping atoms on the surface of AlGaN through the absorption status and current charge density of the transistors was studied. Moreover, the effect of a relative chemical shift between AlGaN and doped hetero clusters of the transistor cell was also investigated. In fact, this article presents the ternary hybrid material of AlGaN as electron carrier after implantation with metalloids (Si, Ge) and metals (Pd, Pt) which introduce deep states into the band gap and high-electron-mobility for application in the transistors.

2. THEORY, MATERIALS AND COMPUTATION

The Si-, Ge-, Pd- or Pt-doped AlGaN nanocage were calculated within the framework of first-principle calculation based on density functional theory (DFT) (Fig. 1) for obtaining the highest short-circuit current density. In Fig. 1, a characteristic special quasirandom supercell structure for AlGaN and (Si, Ge, Pd, Pt)-doped AlGaN containing 17 atoms has been modeled for hydrogen adsorption and formation of hybrid nanomaterials including H–AlGaN and H–(Si, Ge, Pd, Pt)-doped AlGaN with 18 atoms towards energy storage in the transistors [44–49].

The rigid potential energy surface using density functional theory [50–58] was performed due to Gaussian 16 revision C.01 program package [59] and GaussView 6.1 [60]. The coordination input for energy storage on the transistors has applied 6-311+G(d, p) and EPR–3 basis sets. Three factors have been analyzed by means of long-range correction using the Coulomb-attenuating method (CAM), A new hybrid exchange–correlation functional named CAM-B3LYP (Becke–Lee–Yang–Parr) is proposed. The CAM-B3LYP functional comprises of 0.19 Hartree–Fock (HF) plus 0.81 Becke 1988 (B88) exchange interaction at short-range, and 0.65 HF plus 0.35 B88 at long-range [61]. Moreover, Grimme's popular DFT-D3 approach for the treatment of London-dispersion interactions has been used with computational effi-

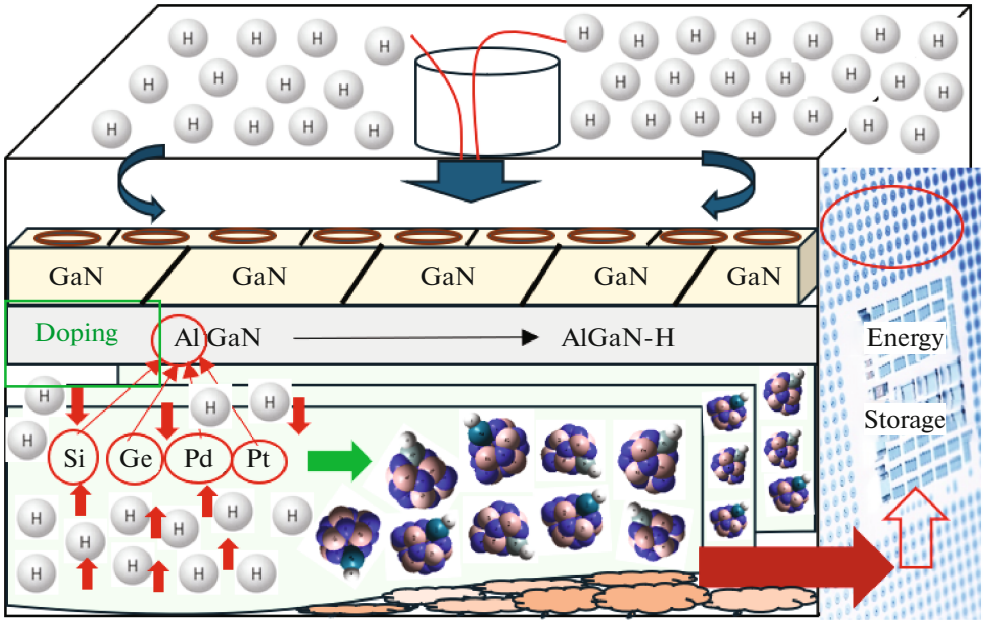

Fig. 1. Application of hetero-clusters of AlGaN, Si–AlGaN, Ge–AlGaN, Pd–AlGaN, and Pt–AlGaN for hydrogen storage in transistors using CAM–B3LYP–D3/6-311+G (d, p) calculation.

ciency and robustness across the periodic table, which makes this approach particularly valuable for the treatment of large systems [62].

Figure 1 shows the process of energy storage on hetero-clusters of AlGaN, Si–AlGaN, Ge–AlGaN, Pd–AlGaN or Pt–AlGaN which are varied to maximize the hydrogen absorption in the active region. Furthermore, we optimized the hydrated nanoclusters including AlGaN–H with multiplicity = 1 and convergence = 0.20, and Si–AlGaN–H, Ge–AlGaN–H, Pd–AlGaN–H, Pt–AlGaN–H with multiplicity = 2 and convergence = 0.98, 0.38, 0.85, 0.88, respectively, through Gaussian 16 revision C.01 program package [59] (Fig. 2). Moreover, overlap integral (S^2) after annihilation for theses hybrid doped materials have been achieved as:

$$S^2_{\text{Si–AlGaN–H}} = 1.6590,\quad S^2_{\text{Ge–AlGaN–H}} = 3.7205,$$
$$S^2_{\text{Pd–AlGaN–H}} = 2.0793,\quad S^2_{\text{Pt–AlGaN–H}} = 2.6350.$$

In isolated system (such as molecule), the energy levels are discrete, the concept of density of state (DOS) is supposed completely valueless in this situation. Therefore, the original total DOS (TDOS) of isolated system can be written as [63]:

$$\text{TDOS}(E) = \sum_i \delta(E - \epsilon_i), \qquad (1)$$

where $\{\epsilon\}$ is eigenvalue set of single-particle Hamilton, δ is Dirac delta function. If δ is replaced by broadening function $F(x)$, such as Gaussian, Lorentzian and pseudo-Voigt function, we get broadened TDOS. The normalized Gaussian function is defined as:

$$G(x) = \frac{1}{c\sqrt{2\pi}} e^{-\frac{x^2}{2c^2}} \quad \text{where} \quad c = \frac{\text{FWHM}}{2\sqrt{2\ln x}}. \qquad (2)$$

Full width at half maximum (FWHM) is an adjustable parameter in Multiwfn. The larger FWHM the TDOS graph looks smoother, and analysis is easier to perform, but more fine-structure is masked. Furthermore, a type of scalar fields called electron localization function (ELF) may demonstrate a broad span of bonding samples. Nevertheless, the distinction between deduced/raised electron delocalization/localization into cyclic π-conjugated sets stays encouraging for ELF [64]. The grosser the electron localization is in an area, the more likely the electron movement is restricted within it. Therefore, they might be discerned from the ones away if electrons are totally centralized. As Bader investigated, the zones with large electron localization possess extensive magnitudes of Fermi hole integration. But, with having a six-dimension function for the Fermi hole, it seems hard to be studied directly. Then, Becke and Edgecombe remarked that spherically averaged like spin conditional pair probability possesses a direct correlation with the Fermi hole and proposed the parameter of electron localization function (ELF) in Multiwfn program [63] and popularized for spin-polarized procedure [65]:

$$\text{ELF}(r) = \frac{1}{1 + [D(r)/D_0(r)]}, \qquad (3)$$

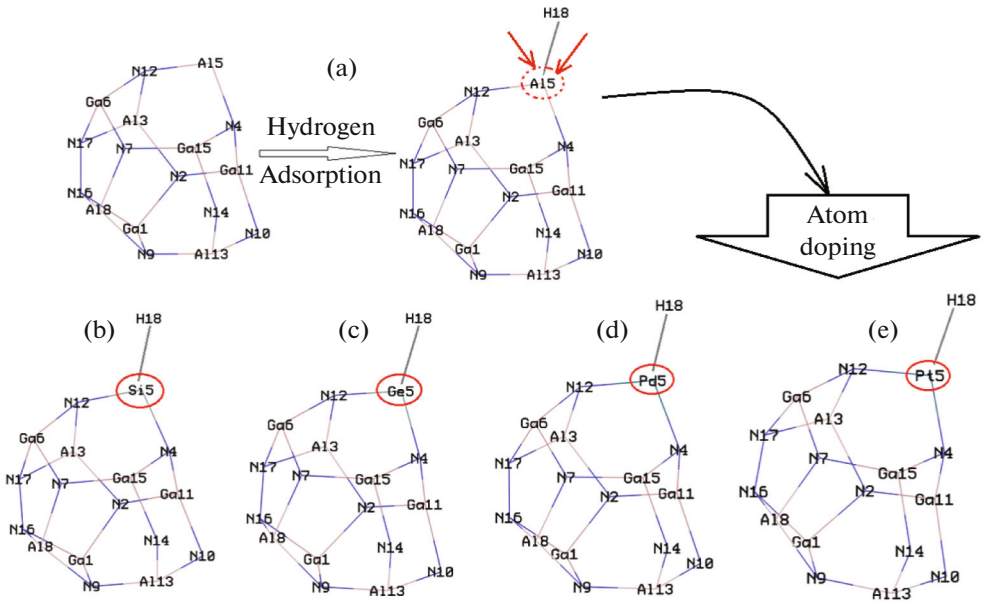

Fig. 2. Characterization of optimized hydrated nanohybrids of (a) AlGaN–H, (b) Si–AlGaN, (c) Ge–AlGaN, (d) Pd–AlGaN, and (e) Pt–AlGaN using Gaussian program Gaussian 16 revision C.01 program package [59].

where

$$D(r) = \frac{1}{2}\sum_i \eta_i |\nabla\varphi_i(r)|^2 - \frac{1}{8}\left[\frac{|\nabla\rho_\alpha(r)|^2}{\rho_\alpha(r)} + \frac{|\nabla\rho_\beta(r)|^2}{\rho_\beta(r)}\right], \quad (4)$$

and

$$D_0(r) = \frac{3}{10}\left(6\pi^2\right)^{2/3}\left[\rho_\alpha(r)^{5/3} + \rho_\beta(r)^{5/3}\right]. \quad (5)$$

For close-shell system, since $\rho_\alpha = \rho_\beta = (1/2)\rho$, D and D_0 terms can be simplified as:

$$D(r) = \frac{1}{2}\sum_i \eta_i |\nabla\varphi_i(r)|^2 - \frac{1}{8}\frac{|\nabla\rho(r)|^2}{\rho(r)}, \quad (6)$$

and

$$D_0(r) = (3/10)\left(3\pi^2\right)^{2/3}\rho(r)^{5/3}. \quad (7)$$

Regarding kinetic energy, ELF was rechecked to be more punctual for both Kohn–Sham DFT and post-HF wavefunctions [66]. In fact, the excess kinetic energy density caused by Pauli repulsion was unfolded by $D(r)$ and $D_0(r)$ may be inspected as Thomas–Fermi kinetic energy density. Because $D_0(r)$ is brough forward the ELF as origin, what the ELF shows is an affiliate localization.

3. RESULTS AND DISCUSSION

3.1. Analysis of CDD, TDOS and ELF

The amounts of charge density differences "CDD" is measured by considering isolated atoms or noninteracting ones. The mentioned approximation can be the lightest to use because the superposition value may be received from the primary status of the self-consistency cycle in the code that carries out the density functional theory (Figs. 3a–3e) [67]. In Fig. 3a, the atoms of Al5, H18 accompanying nitrogen and gallium atoms from AlGaN and AlGaN–H, respectively have shown the fluctuation around –9 to +3 Bohr. The atoms of Si5, H18 accompanying aluminum, gallium and nitrogen from Si–AlGaN/Si–AlGaN–H, respectively have indicated the fluctuation around –9 to +3 Bohr (Fig. 3b). However, the atoms of Ge5, H18 accompanying aluminum, gallium and nitrogen from Ge–AlGaN and Ge–AlGaN–H have indicated the fluctuation around –9 to + 5 Bohr and –9 to +7 Bohr, respectively (Fig. 3c). For two nanoclusters of Pd–AlGaN (Fig. 3d) and Pt–AlGaN (Fig. 3e), it was observer the fluctuation around –9 to –1 Bohr for aluminum, gallium and nitrogen and Pd5 or Pt5 and H18 before H-adsorption and between –9 to +6 Bohr after H-adsorption. To better understand the different adsorption characteristics of AlGaN–H, Si–AlGaN–H, Ge–AlGaN–H, Pd–AlGaN–H, and Pt–AlGaN–H, total density of states (TDOS) using Multiwfn program [63] has been measured. This parameter can indicate the existence of important chemical interactions often on the convex side (Figs. 4a–4e).

In the TDOS map, each discrete vertical line corresponds to a molecular orbital (MO), the dashed line highlights the position of HOMO. The curve is the TDOS simulated based on the distribution of MO energy levels. In the negative part, the region around –0.30 a.u. has obviously larger state density than other regions for AlGaN–H, Si–AlGaN–H, Ge–AlGaN–H, Pd–AlGaN–H, and Pt–AlGaN–H (Figs. 4a–4e).

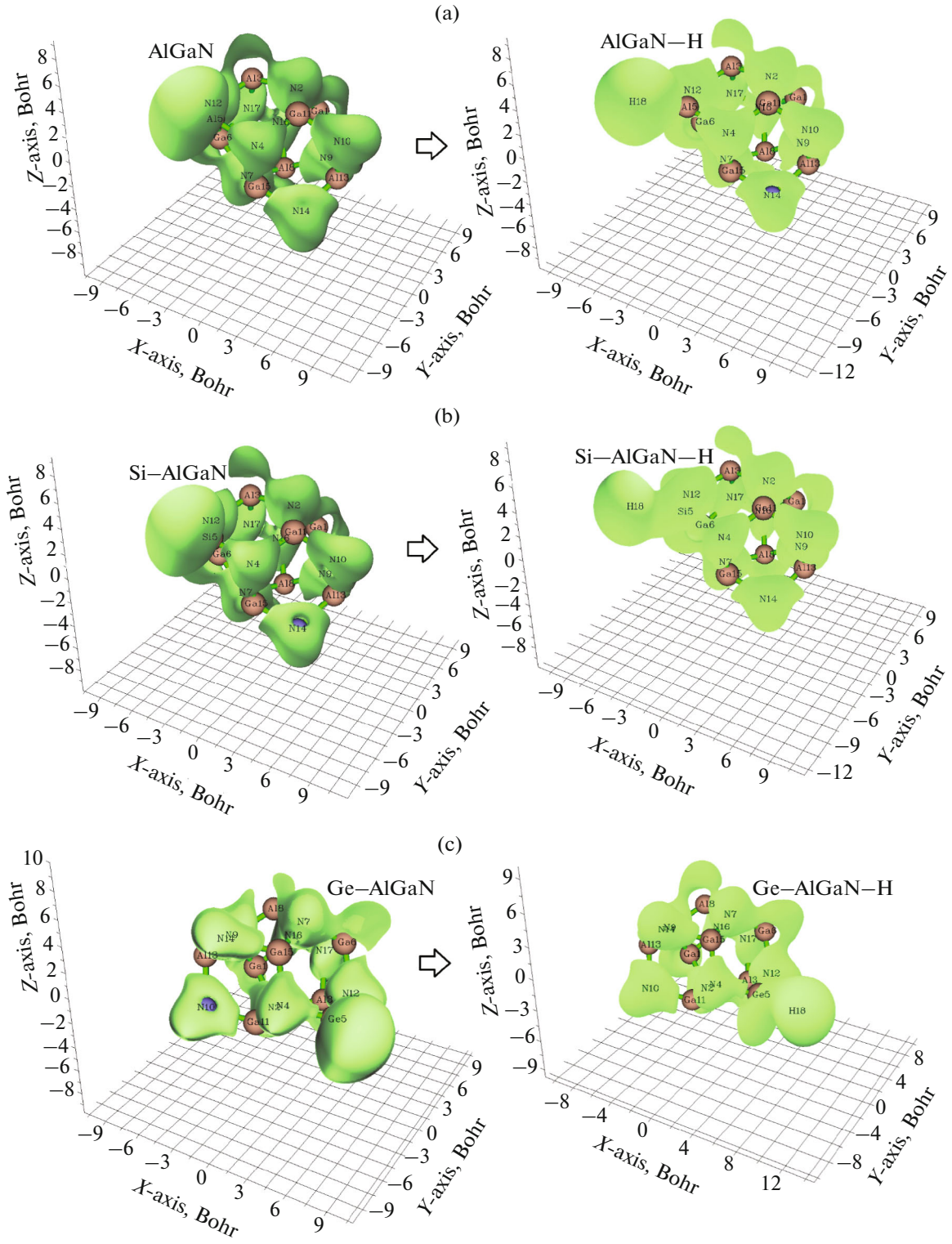

Fig. 3. CDD graphs for hetero-clusters through hydrogen adsorption including (a) AlGaN/AlGaN–H, (b) Si–AlGaN/Si–AlGaN–H, (c) Ge–AlGaN/Ge–AlGaN–H, (d) Pd–AlGaN/Pd–AlGaN–H, and (e) Pt–AlGaN/Pt–AlGaN–H.

However, Pd–AlGaN–H (Fig. 4e) and Pt–AlGaN–H (Fig. 4d) have shown larger state density than Si–AlGaN–H (Fig. 4b), Ge–AlGaN–H (Fig. 4c) and AlGaN–H (Fig. 4a). It is remarkable that the excessive growth technique on doping palladium or platinum as noble transition metals is a potential approach

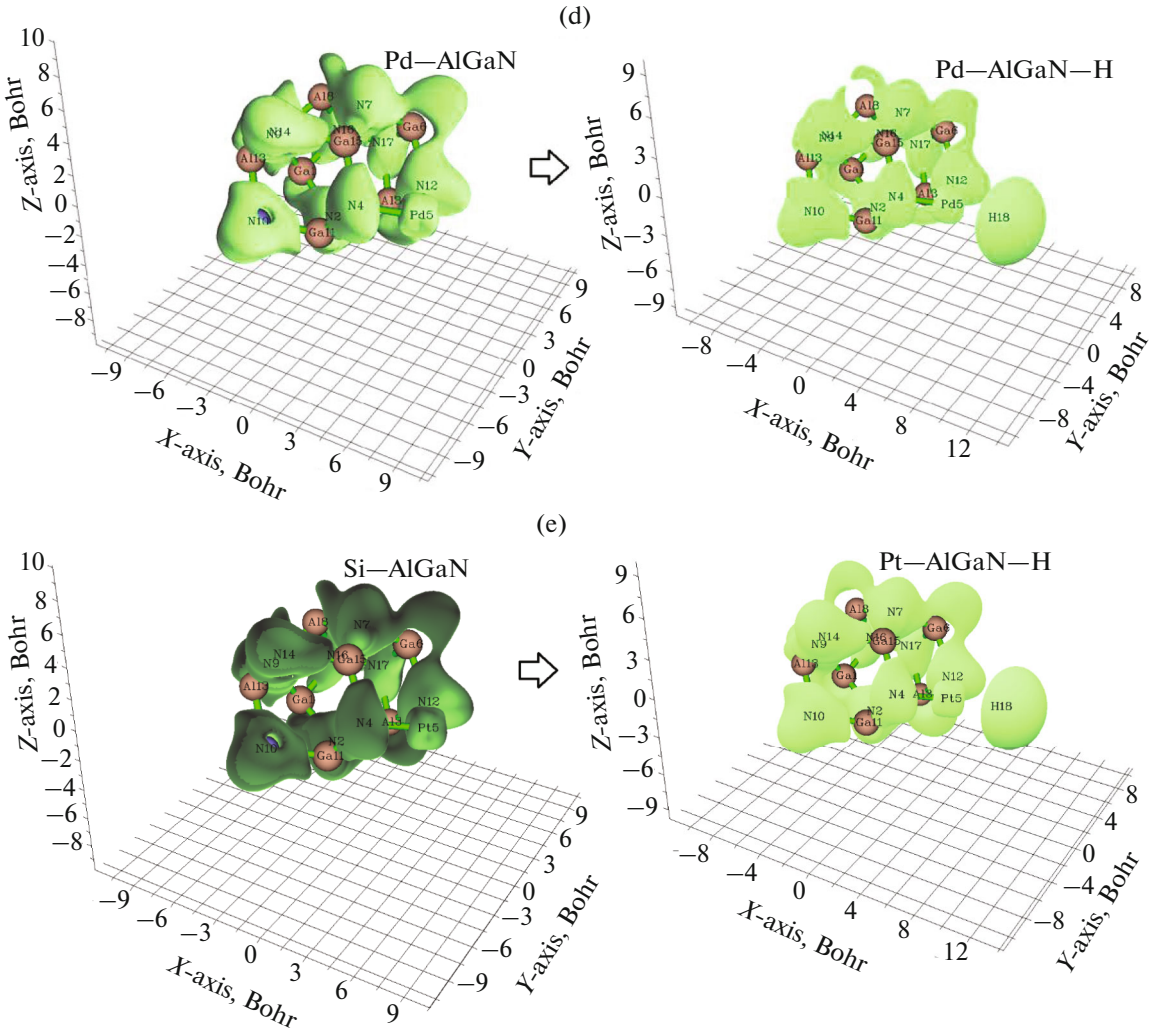

Fig. 3. (Contd.)

to designing high efficiency hybrid semipolar gallium nitride devices on palladium or platinum layers in a long wavelength zone [68].

The compounds of AlGaN–H, Si–AlGaN–H, Ge–AlGaN–H, Pd–AlGaN–H, and Pt–AlGaN–H can be defined by ELF graphs owing to exploring their delocalization/localization characterizations of electrons and chemical bonds (Figs. 5a–5e).The counter map of ELF for AlGaN–H has shown the electron delocalization due to labeling atoms of N4, Al5, H18 (Fig. 5a). Then, hydration of Si- and Ge-doped AlGaN indicates a larger isosurface map of electron delocalization due to labeling atoms of N4, Si5, H18 of Si–AlGaN–H (Fig. 5b) and N4, Ge5, H18 of Ge–AlGaN–H (Fig. 5c). A vaster jointed area engaged by an isosurface map for Pd and Pt doping AlGaN towards formation of hetero-clusters of Pd–AlGaN–H (Fig. 5d) and Pt–AlGaN–H (Fig. 5e) after hydrogen adsorption due to labeling atoms of N4, Pd/Pt5, H18, respectively. A narrower connected area occupied by an isosurface map means that electron delocalization is relatively difficult. However, the large counter map of ELF for Pt–AlGaN, Pd–AlGaN–H, Si–AlGaN, Ge–AlGaN can confirm that doping Pd, Pt, Si, Ge nanoparticles on the surface, increases the efficiency of ternary transistor cell of AlGaN for energy storage. Besides, the changes of charge density analysis have illustrated that AlGaN has shown the Bader charge of –1.272 coulomb, and after doping with silicon, germanium, palladium, platinum has indicated the Bader charge of –1.290, –1.285, –1.292, –1.309 coulomb for Si–AlGaN, Ge–AlGaN, Pd–AlGaN, Pt–AlGaN, respectively, that describes the tensity value of these hetero-clusters for energy storage (Table 1).

3.2. Analysis of Nuclear Magnetic Resonance Spectra

Based on the resulted amounts, nuclear magnetic resonance (NMR) spectra of Si–AlGaN, Ge–

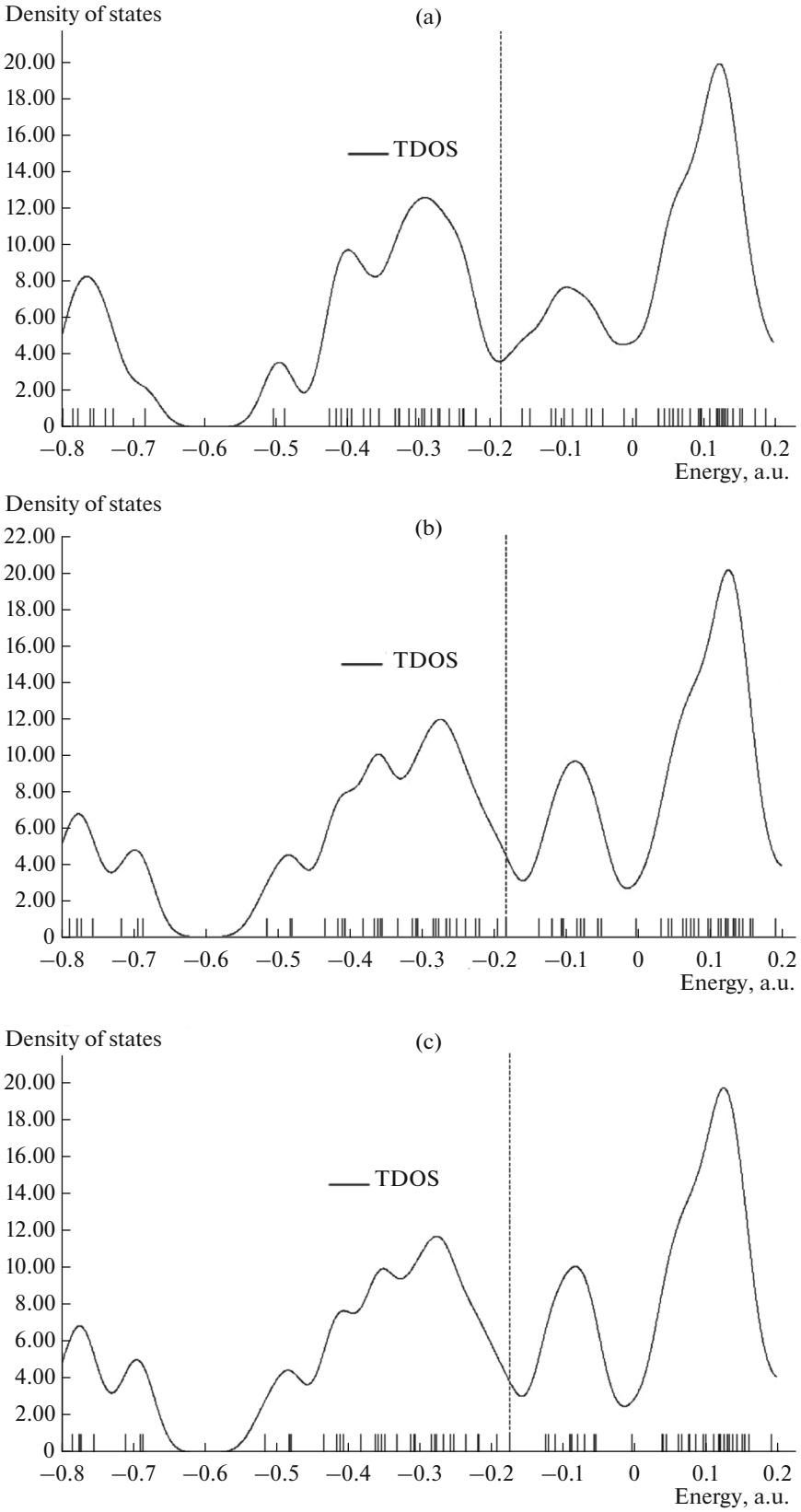

Fig. 4. TDOS graphs of hetero-clusters include (a) AlGaN–H, (b) Si–AlGaN–H, (c) Ge–AlGaN–H, (d) Pd–AlGaN–H, and (e) Pt–AlGaN–H.

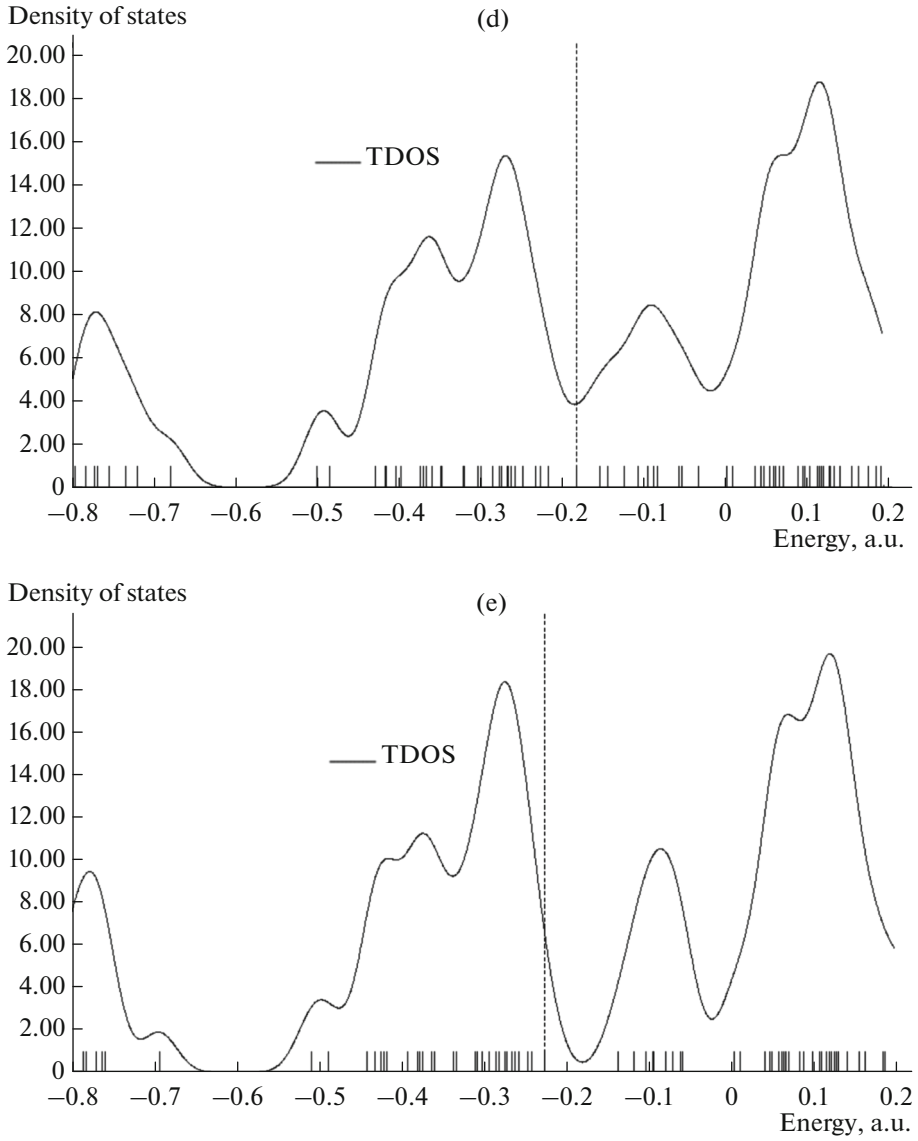

Fig. 4. (Contd.)

AlGaN, Pd–AlGaN, Pt–AlGaN hetero-clusters as the potential molecules for energy storage can unravel the efficiency of these complexes in transistors. From the DFT calculations, it has been attained the chemical shielding (CS) tensors in the principal axes system to estimate the isotropic chemical-shielding (CSI) and anisotropic chemical-shielding (CSA) [69]:

$$\sigma_{iso} = (\sigma_{11} + \sigma_{22} + \sigma_{33})/3, \quad (8)$$

$$\sigma_{aniso} = \sigma_{33} - (\sigma_{22} + \sigma_{11})/2. \quad (9)$$

The NMR data of isotropic (σ_{iso}) and anisotropic shielding tensors (σ_{aniso}) for ternary alloy of AlGaN and doped hetero-clusters of Si–AlGaN, Ge–AlGaN, Pd–AlGaN, Pt–AlGaN through hydrogen adsorption have been computed by Gaussian 16 revision C.01 program package [59] and been shown in Table 2. The notable fragile signal intensity close to the parallel edge of the nanocluster sample might be owing to silicon or germanium binding induced non-spherical distribution of Si–AlGaN (Fig. 6a) or Ge–AlGaN (Fig. 6b) hetero-clusters. Figures 6c, 6d) exhibited the same tendency of shielding for palladium or platinum; however, a considerable deviation exists from doping atoms of palladium or platinum as electron acceptors on the surface of Pd–AlGaN or Pt–AlGaN hetero-clusters.

The observed increase in the chemical shift anisotropy spans for nanocages of Si–AlGaN/Si–AlGaN–H (Fig. 6a) and Ge–AlGaN/Ge–AlGaN–H (Fig. 6b) is near N10, N14, N17. The yield of electromagnetic shifting can be directed by the mentioned active nitrogen atoms extracted from ternary hybrid hereto-clusters. It has shown that the intensity for energy storage

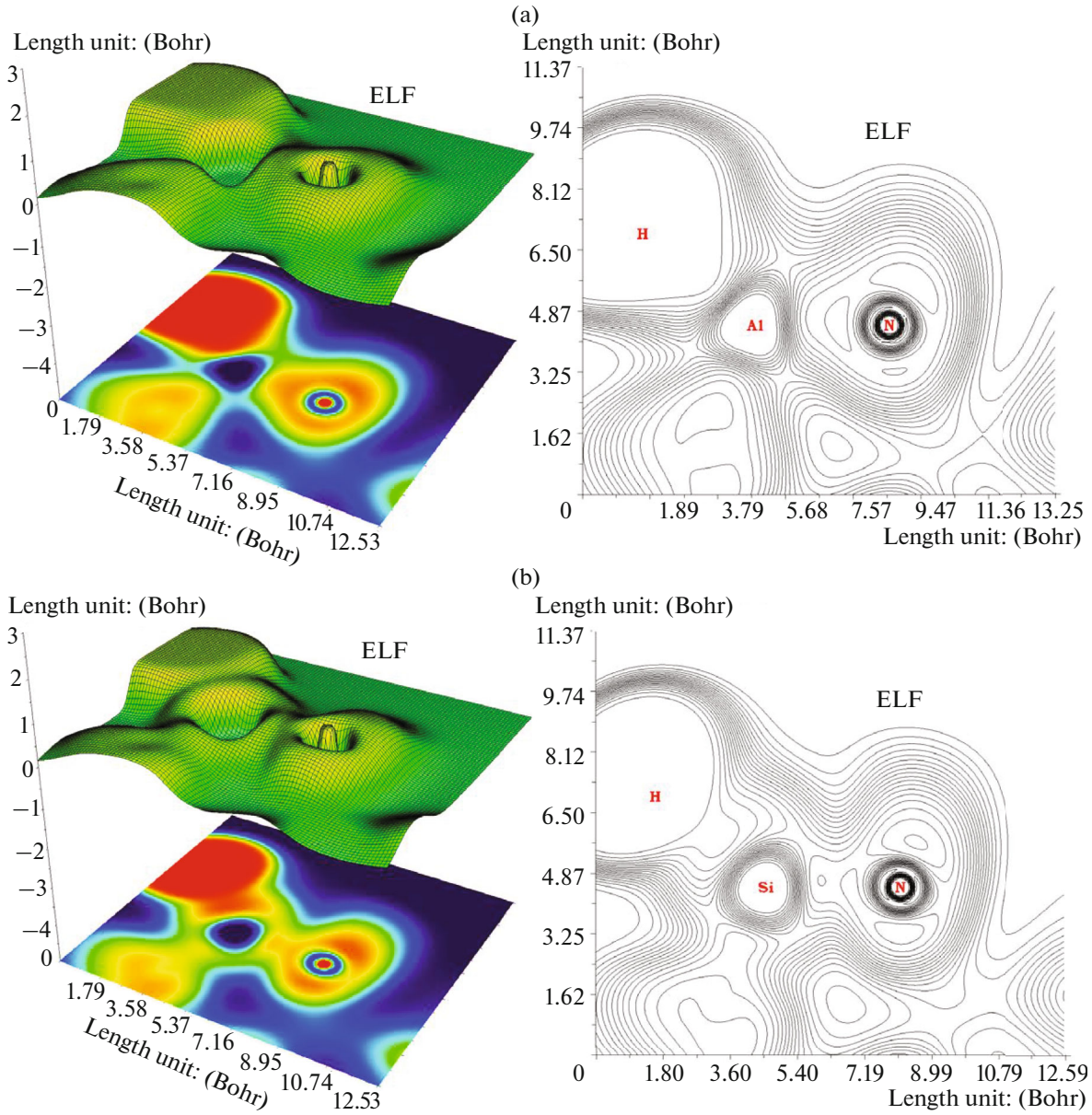

Fig. 5. The graphs of ELF for hetero-clusters include (a) AlGaN–H, (b) Si–AlGaN–H, (c) Ge–AlGaN–H, (d) Pd–AlGaN–H, and (e) Pt–AlGaN–H. (Counter line map in the right and shaded surface map with projection in the left).

can be enhanced in Pd–AlGaN (Fig. 6c) and Pt–AlGaN (Fig. 6d) through hydration and formation of Pd–AlGaN–H and Pt–AlGaN–H due to oscillating of chemical shielding in N10, N14, N16, N17 atoms. So, it can be observed that doped hetero-clusters of Si–AlGaN, Ge–AlGaN, Pd–AlGaN, Pt–AlGaN might ameliorate the capability of AlGaN in transistors for energy storage.

The local magnetic moment of NiN4 makes the primary contribution. The doped Si, Ge, Pd, Pt atoms with their nearby N4, N7, N12 atoms (Fig. 2) in hybrid materials of Si–AlGaN, Ge–AlGaN, Pd–AlGaN, Pt–AlGaN, then N atoms are spin polarized and couple with Si, Ge, Pd, Pt atoms, which result in magnetism. Therefore, the p-d exchange mechanism is responsible for magnetism in (Si, Ge, Pd, Pt)-doped AlGaN which can make it possible to the applications for the spin electric devices (Figs. 6a–6d).

3.3. Insight of Infrared Spectroscopy and Thermochemistry

The infrared spectroscopy (IR) has been performed for ternary nanocage of AlGaN (Fig. 7a) and hybrid alloys of Si–AlGaN (Fig. 7b), Ge–AlGaN (Fig. 7c), Pd–AlGaN (Fig. 7d), Pt–AlGaN (Fig. 7e)

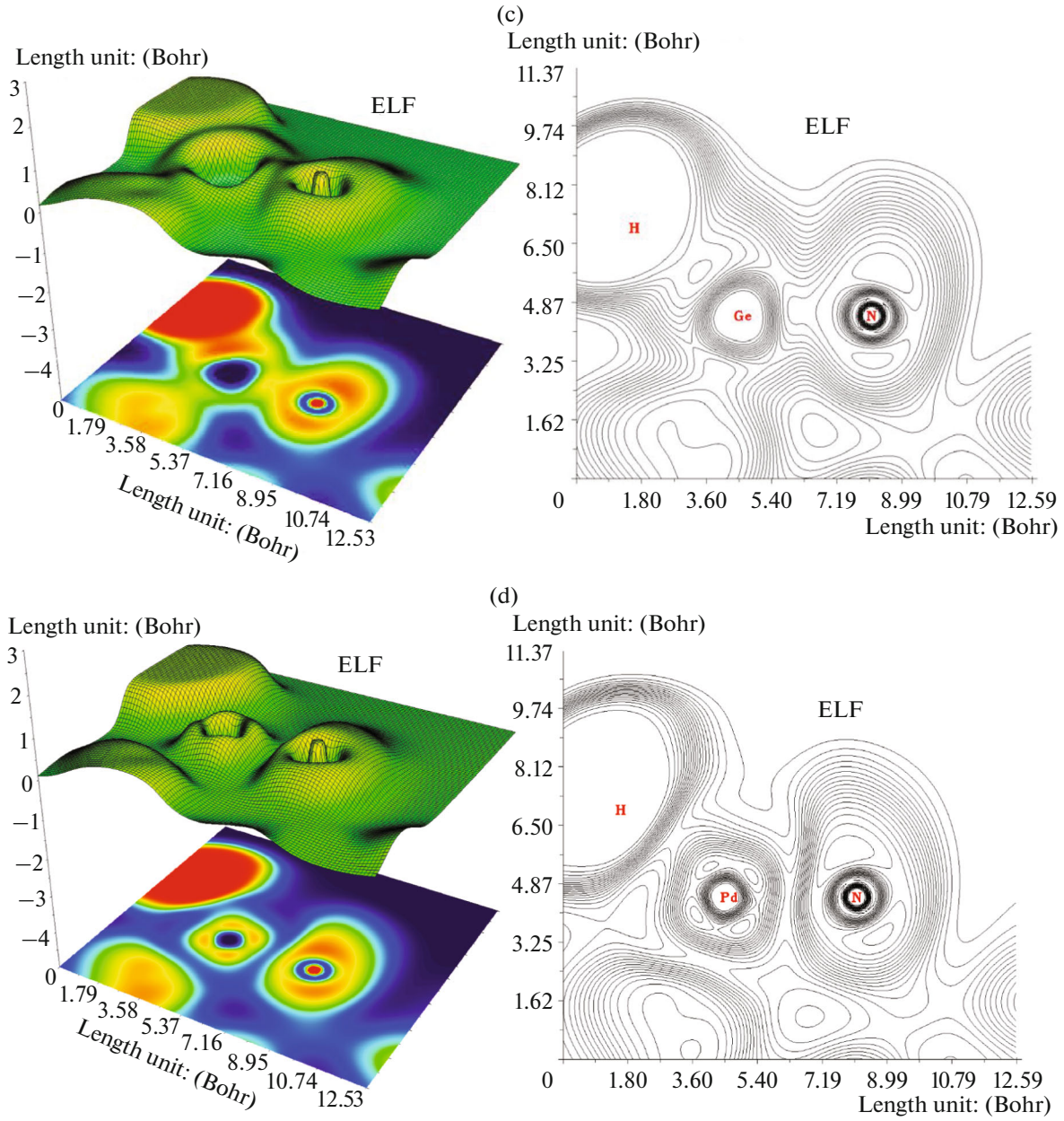

Fig. 5. (Contd.)

through hydrogen adsorption. The frequency values through the IR curves between 100–1000 cm^{-1} have been achieved for AlGaN–H with several peaks with the highest intensity around 396.73, 705.98,793.75, 941.91 cm^{-1} (Fig. 7a). Figure 7b shows the frequency range between 100–800 cm^{-1} for Si–AlGaN–H with peaks with the highest intensity around 388.35, 403.32 and 606.23 cm^{-1}. Figure 7c has indicated the fluctuation of frequency between 100–800 cm^{-1} for Ge–AlGaN–H with strong and peaks with the highest intensity around 399.71, 444.26, and 696.52 cm^{-1}. The graph of Fig. 7d has been observed in the frequency range between 100–800 cm^{-1} for Pd–AlGaN–H with several peaks with the highest intensity around 391.43, 477.43, 641.08 and 728.76 cm^{-1}. Furthermore, the graph of Fig. 7e has been observed in the frequency range between 100–800 cm^{-1} for Pt–AlGaN–H with several peaks with the highest intensity around 405.90, 433.01, 646.34, 674.46, and 722.73 cm^{-1}.

Energy storage with hetero-clusters has described that the frame of the overcoming cluster is related to Pt–AlGaN or Pd–AlGaN in the high amounts of frequency. This property makes Pt–AlGaN or Pd–AlGaN potentially advantageous for certain high-fre-

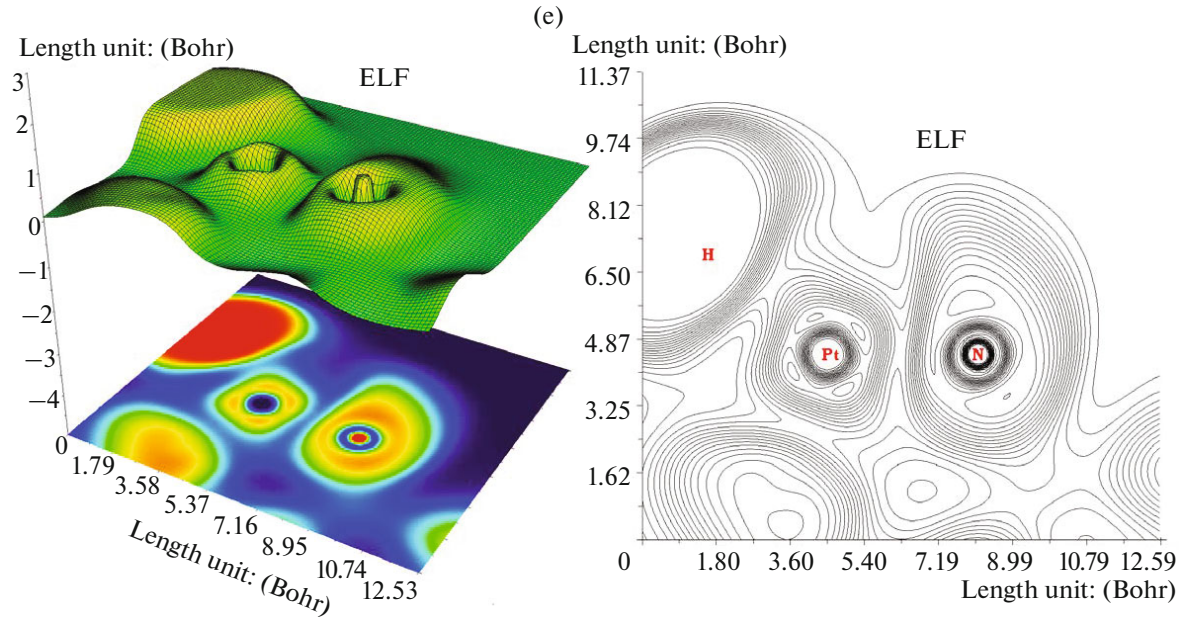

Fig. 5. (Contd.)

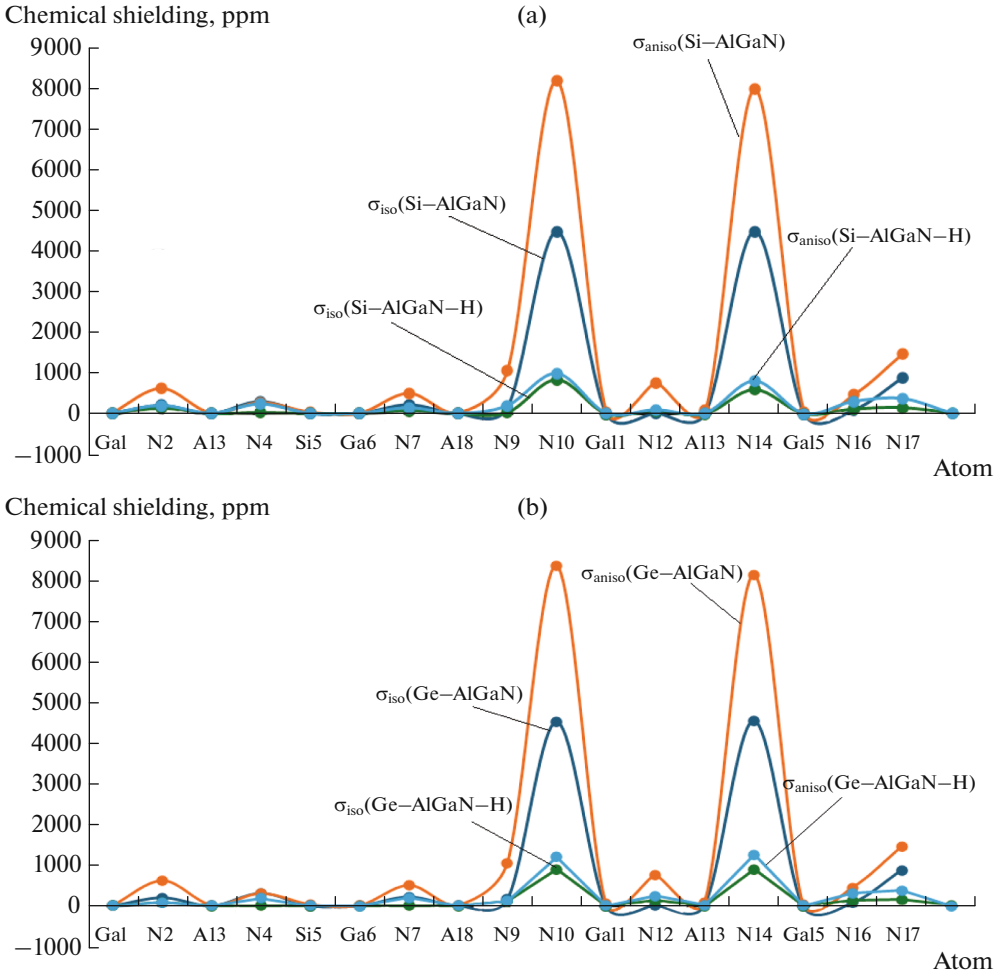

Fig. 6. The NMR spectra for hetero-clusters of (a) Si–AlGaN/Si–AlGaN–H, (b) Ge–AlGaN/Ge–AlGaN–H, (c) Pd–AlGaN/Pd–AlGaN–H, (d) Pt–AlGaN/Pt–AlGaN–H.

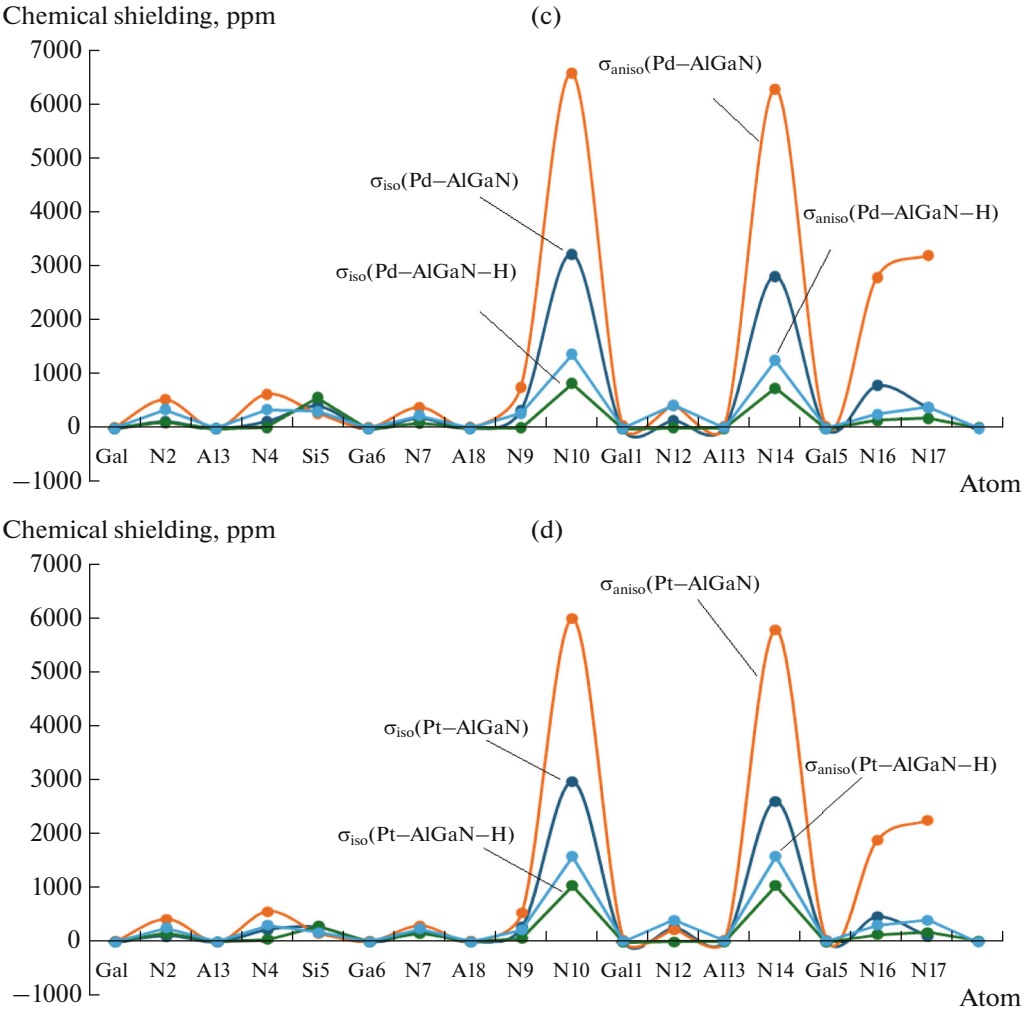

Fig. 6. (Contd.)

quency applications requiring transistor cells for energy storage. The advantages of platinum or palladium over aluminum gallium nitride include its higher electron and hole mobility, allowing platinum or palladium doping devices to operate at higher frequencies than silicon or germanium doping devices. Table 3 through the thermodynamic specifications concluded that hetero-clusters of AlGaN, Si–AlGaN, Ge–AlGaN, Pd–AlGaN, or Pt–AlGaN might be more efficient structure for energy storage in the transistor cells. Figure 7 has taught that the doping atom on the AlGaN induces a broadening of the frequency and intensity as well as the stability energy in the alloy. Also, considering *d*-orbitals in Ge, Pd, Pt against p-orbitals in Al and Si, it is observed a widening of the absorption peak in Figs. 7a, 7b) and Figs. 7c–7e), respectively.

Thermodynamic parameters of hetero-clusters of AlGaN/AlGaN–H, Si–AlGaN/Si–AlGaN–H, Ge–AlGaN/Ge–AlGaN–H, Pd–AlGaN/Pd–AlGaN–H, and Pt–AlGaN/Pt–AlGaN–H have been assigned (Table 3). The changes of Gibbs free energy versus dipole moment could detect the maximum efficiency of Pd–AlGaN–H and Pt–AlGaN–H hetero-clusters for energy storage in the transistor cells through ΔG^{o}_{ads}. The adsorption efficiency of AlGaN–H, Si–AlGaN–H, Ge–AlGaN–H, Pd–AlGaN–H, and Pt–AlGaN–H based on dipole moment has been evaluated by the ΔG^{o}_{ads}. The transistor cells formed by AlGaN, Si–AlGaN, Ge–AlGaN, Pd–AlGaN, and Pt–AlGaN feature a hierarchical structure with the electron donor/acceptor layer sandwiched by anode and cathode, which raises the importance of controlling the molecular crystal orientation, domain size, and vertical distribution to facilitate the charge collection at electrodes [70–78]. The doping obviously reduces aluminum atoms composition, the aggregation of Al–Al and induces the deep energy level. This greatly decreases the defects and improves the valence band potential of AlGaN nanorods. We concluded that the thermochemical properties in 298 K are

Table 1. Data of Bader charge (Q/Coulomb) for selected atoms of Si–AlGaN, Si–AlGaN–H, Ge–AlGaN, Ge–AlGaN–H, Pd–AlGaN, Pd–AlGaN–H, Pt–AlGaN, Pt–AlGaN–H hetero-clusters

Si–AlGaN		Si–AlGaN–H		Ge–AlGaN		Ge–AlGaN–H	
atom	*Q*	atom	*Q*	atom	*Q*	atom	*Q*
Ga1	1.0145	Ga1	0.9919	Ga1	1.0106	Ga1	0.9784
N2	−1.1427	N2	−1.1462	N2	−1.1420	N2	−1.1475
Al3	1.2522	Al3	1.2832	Al3	1.2476	Al3	1.2976
N4	−1.1045	N4	−1.0695	N4	−1.0930	N4	−1.0819
Si5	0.7566	Si5	0.7501	Ge5	0.7604	Ge5	0.6899
Ga6	0.9752	Ga6	0.9583	Ga6	0.9708	Ga6	0.9852
N7	−1.1268	N7	−1.1213	N7	−1.1269	N7	−1.1483
Al8	1.2902	Al8	1.2802	Al8	1.2854	Al8	1.2668
N9	−1.1861	N9	−1.1838	N9	−1.1864	N9	−1.2073
N10	−0.7902	N10	−0.7725	N10	−0.7894	N10	−0.7707
Ga11	1.0153	Ga11	1.0639	Ga11	1.0092	Ga11	1.0702
N12	−1.1390	N12	−1.1318	N12	−1.1251	N12	−1.1185
Al13	1.1938	Al13	1.2028	Al13	1.1914	Al13	1.2308
N14	−0.7775	N14	−0.8328	N14	−0.7773	N14	−0.7833
Ga15	1.0280	Ga15	1.0092	Ga15	1.0223	Ga15	1.0407
N16	−0.6448	N16	−0.6320	N16	−0.6448	N16	−0.6289
N17	−0.6142	N17	−0.6327	N17	−0.6129	N17	−0.6330
		H18	−0.0174			H18	−0.0401
Pd–AlGaN		Pd–AlGaN–H		Pt–AlGaN		Pt–AlGaN–H	
atom	*Q*	atom	*Q*	atom	*Q*	atom	*Q*
Ga1	1.0197	Ga1	1.0144	Ga1	1.0296	Ga1	1.0120
N2	−1.1542	N2	−1.1640	N2	−1.1551	N2	−1.1543
Al3	1.2464	Al3	1.2954	Al3	1.2607	Al3	1.2596
N4	−0.8860	N4	−0.9111	N4	−0.9550	N4	−1.0208
Pd5	0.3351	Pd5	0.1988	Pt5	0.4083	Pt5	0.2914
Ga6	0.9649	Ga6	0.9996	Ga6	0.9764	Ga6	0.9953
N7	−1.1344	N7	−1.1330	N7	−1.1356	N7	−1.1495
Al8	1.2922	Al8	1.3138	Al8	1.3086	Al8	1.2820
N9	−1.1921	N9	−1.1890	N9	−1.1911	N9	−1.2098
N10	−0.8065	N10	−0.7750	N10	−0.8109	N10	−0.7700
Ga11	1.0388	Ga11	1.0760	Ga11	1.0590	Ga11	1.0862
N12	−0.9359	N12	−0.9211	N12	−1.0113	N12	−0.9789
Al13	1.2001	Al13	1.2236	Al13	1.2068	Al13	1.2564
N14	−0.7799	N14	−0.8321	N14	−0.7850	N14	−0.7735
Ga15	1.0385	Ga15	1.0614	Ga15	1.0583	Ga15	1.0974
N16	−0.6380	N16	−0.6337	N16	−0.6441	N16	−0.6373
N17	−0.6087	N17	−0.6319	N17	−0.6196	N17	−0.6264
		H18	0.0080			H18	0.0402

Table 2. Data of NMR shielding tensors (ppm) for selected atoms of Si–AlGaN, Si–AlGaN–H, Ge–AlGaN, Ge–AlGaN–H, Pd–AlGaN, Pd–AlGaN–H, Pt–AlGaN, Pt–AlGaN–H hetero-clusters

Si–AlGaN			Si–AlGaN–H			Ge–AlGaN			Ge–AlGaN–H		
Atom	σ_{iso}	σ_{aniso}	Atom	σ_{iso}	σ_{aniso}	Atom	σ_{iso}	σ_{aniso}	Atom	σ_{iso}	σ_{aniso}
Ga1	12.3013	19.4796	Ga1	8.6544	9.1405	Ga1	12.3701	19.4552	Ga1	9.5050	8.1078
N2	211.7163	624.2011	N2	139.8648	203.1463	N2	210.7415	620.2692	N2	87.4120	93.0730
Al3	11.8826	23.1616	Al3	7.5097	11.2847	Al3	11.8697	22.2821	Al3	5.7319	8.0769
N4	308.1022	275.8609	N4	36.9963	240.3280	N4	319.5534	305.1407	N4	8.2332	198.1721
Si5	18.2189	43.6183	Si5	6.8277	6.9751	Ge5	6.4054	35.0759	Ge5	2.0323	8.8999
Ga6	12.0787	12.6380	Ga6	9.2800	9.1124	Ga6	12.1568	12.7906	Ga6	5.2376	6.8459
N7	228.8424	504.8396	N7	82.7523	146.7660	N7	228.9795	505.9304	N7	16.9463	207.2039
Al8	10.7942	23.4651	Al8	8.7754	9.3173	Al8	10.9741	23.1125	Al8	7.5526	8.1068
N9	169.8457	1065.9161	N9	33.3772	201.2094	N9	173.7625	1066.8591	N9	113.2047	123.9299
N10	4464.2852	8163.3854	N10	842.2081	996.9161	N10	4523.8020	8361.7121	N10	904.7856	1211.6541
Ga11	3.6161	52.5220	Ga11	3.4073	16.3894	Ga11	3.3168	53.5359	Ga11	1.3365	11.3798
N12	26.9395	761.3443	N12	73.4276	95.9736	N12	24.4903	753.6545	N12	142.5351	248.7533
Al13	25.8378	86.3375	Al13	0.3668	13.3565	Al13	26.6926	88.2322	Al13	3.0738	21.6141
N14	4470.3899	7959.1467	N14	600.5182	810.9072	N14	4555.6082	8140.9701	N14	905.2174	1261.3064
Ga15	2.0074	49.6996	Ga15	6.3057	6.2622	Ga15	2.2319	50.4376	Ga15	0.6348	10.7545
N16	100.4200	471.6692	N16	120.5887	303.1641	N16	82.8132	452.4308	N16	140.9833	315.6102
N17	898.8804	1478.9510	N17	155.8962	373.8904	N17	887.5771	1455.5907	N17	158.0298	386.8834
			H18	19.9144	7.4406				H18	20.2236	5.1984
Pd–AlGaN			Pd–AlGaN–H			Pt–AlGaN			Pt–AlGaN–H		
atom	σ_{iso}	σ_{aniso}	atom	σ_{iso}	σ_{aniso}	atom	σ_{iso}	σ_{aniso}	atom	σ_{iso}	σ_{aniso}
Ga1	6.3766	18.0028	Ga1	6.0837	9.8634	Ga1	6.7747	16.5908	Ga1	9.0276	8.5410
N2	137.2700	537.0084	N2	119.6542	355.5546	N2	118.0634	425.2258	N2	163.8150	264.9147
Al3	7.8714	8.3978	Al3	4.1601	10.1059	Al3	6.6627	9.1988	Al3	6.2947	8.3839
N4	142.7993	640.3753	N4	25.3590	352.2755	N4	235.1193	569.0172	N4	53.6903	313.0248
Pd5	425.0297	289.9913	Pd5	579.5696	326.7124	Pt5	279.6570	164.2323	Pt5	297.6406	187.3574
Ga6	7.5755	22.4485	Ga6	4.5484	9.9804	Ga6	7.0659	18.4153	Ga6	7.2481	9.0657
N7	200.0622	399.4347	N7	109.9352	244.3252	N7	174.4217	304.4223	N7	164.6688	247.8177
Al8	14.5665	22.6274	Al8	5.7643	12.7993	Al8	11.7895	15.9394	Al8	7.6161	9.3677
N9	345.3133	774.5338	N9	21.1999	292.1086	N9	280.2062	547.5521	N9	67.0777	222.5959
N10	3220.8355	6565.7451	N10	834.5209	1372.6043	N10	2958.6678	5956.8234	N10	1039.1044	1580.1149
Ga11	3.2676	52.6089	Ga11	2.1554	12.3921	Ga11	1.8556	48.2664	Ga11	1.2514	16.3750
N12	153.9286	438.2476	N12	19.9025	433.0358	N12	265.1746	235.3889	N12	5.1458	409.1643
Al13	31.4093	41.7886	Al13	5.4915	15.1180	Al13	29.2394	39.0399	Al13	6.2802	23.9488
N14	2818.5234	6276.4487	N14	753.5016	1263.8175	N14	2596.9745	5751.3361	N14	1043.1971	1585.4470
Ga15	7.6208	51.1369	Ga15	1.2120	9.4616	Ga15	6.7761	46.7202	Ga15	1.6077	17.0100
N16	795.6155	2802.9315	N16	154.7879	274.3394	N16	471.9415	1878.4952	N16	139.5673	310.2036
N17	402.9201	3204.0854	N17	194.6205	396.8113	N17	111.3974	2245.3639	N17	185.5633	407.1062
			H18	23.7627	6.0687				H18	24.2336	4.7693

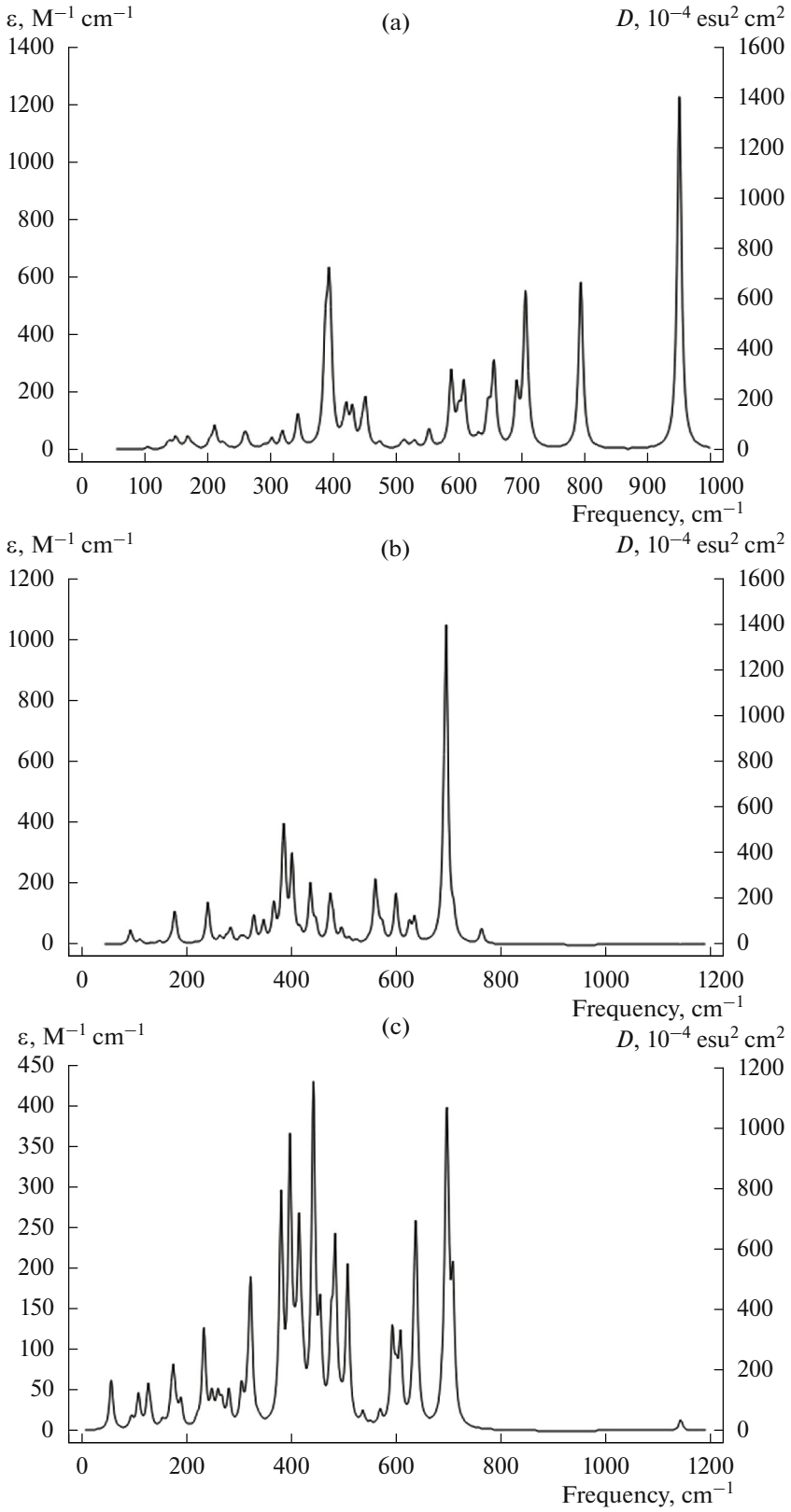

Fig. 7. The Frequency (cm^{-1}) changes through the IR spectra for hetero-clusters of (a) AlGaN–H, (b) Si–AlGaN–H, (c) Ge–AlGaN–H, (d) Pd–AlGaN–H, and (e) Pt–AlGaN–H. [Note: ε (M^{-1} cm^{-1}) is the absorbance unit and D (10^{-4} esu^2 cm^2) is the dipole strength via the esu or electrostatic unit, which is a unit of charge in the cgs (centimeter-gram-second system)].

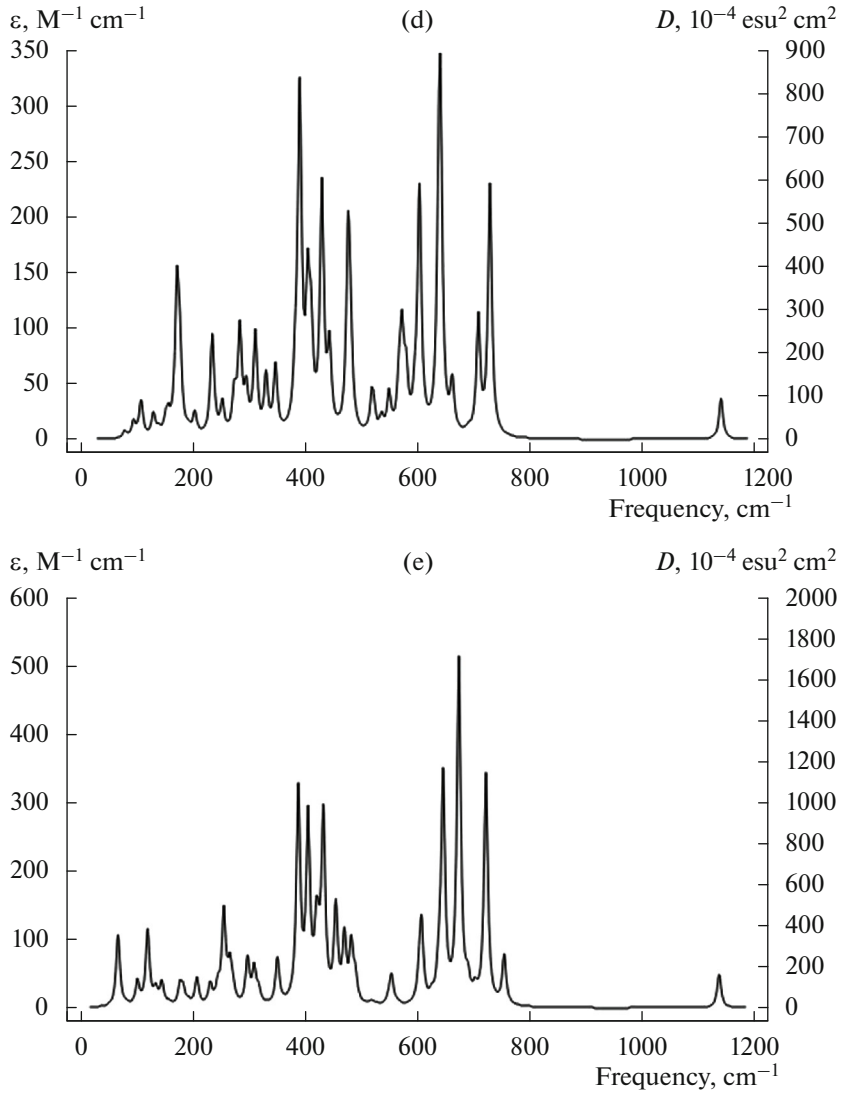

Fig. 7. (Contd.)

Table 3. The thermodynamic characters of AlGaN/AlGaN–H, Si–AlGaN/Si–AlGaN–H, Ge–AlGaN/Ge–AlGaN–H, Pd–AlGaN/Pd–AlGaN–H, and Pt–AlGaN/Pt–AlGaN–H nanoclusters using CAM–B3LYP–D3/6-311+G(d, p) calculation

Compound	Dipole moment, D	$\Delta E^{o}_{ads} \times 10^{-3}$, kcal/mol	$\Delta H^{o}_{ads} \times 10^{-3}$, kcal/mol	$\Delta G^{o}_{ads} \times 10^{-3}$, kcal/mol	$E^{o}_{H-binding}$, kcal/mol
AlGaN	4.6672	–319.178	–319.178	–319.219	–
AlGaN–H	5.5817	–319.503	–319.502	–319.542	–325
Si–AlGaN	5.8081	–320.296	–320.295	–320.335	–
Si–AlGaN–H	5.0608	–320.656	–320.656	–320.697	–360
Ge–AlGaN	5.6442	–320.240	–320.239	–320.279	–
Ge–AlGaN–H	4.3890	–320.608	–320.607	–320.650	–368
Pd–AlGaN	5.1550	–397.327	–397.327	–397.368	–
Pd–AlGaN–H	6.2464	–397.686	–397.686	–397.729	–359
Pt–AlGaN	5.5186	–392.573	–392.573	–392.614	–
Pt–AlGaN–H	5.0840	–392.956	–392.956	–392.999	–383

related to the average micropore size and total pore volume, respectively. These parameters evaluate the enthalpy of adsorption which can be used to assess the best doping atoms for hydrogen storage [79–81].

In this paper, we have demonstrated that the ternary semiconductor of aluminum gallium nitride structure can lead to a significant absorption enhancement in a broad spectral range of incident light in the presence of silicon, germanium, palladium or platinum. A comparison between transistor cells containing 4d and 5d transition metals of Pd and Pt, respectively, doped AlGaN shows that a transistor containing these elements show a more enhanced cell performance than the cells containing only the bare AlGaN structure. This efficient doping strategy not only bridges the gaps of heteroatom doped AlGaN based semiconductor materials, but also can provide deep insights into controlling the electrical and optical properties of these doping hybrid nanoclusters.

CONCLUSIONS

We have provided a ternary semiconductor of aluminum gallium nitride transistors which is doped with silicon, germanium, palladium or platinum. Then, hydrogen grabbing on the hetero-clusters of AlGaN, Si–AlGaN, Ge–AlGaN, Pd–AlGaN, and Pt–AlGaN as transistor cells was investigated by DFT method. The geometrical parameters of doping atoms on the surface of AlGaN through the absorption status and current charge density of the transistor cells was studied. Moreover, the effect of a relative chemical shift between AlGaN and doped hetero clusters of the transistor cell was also investigated. Thermodynamic parameters have constructed a detailed molecular model for atom–atom interactions and a distribution of point charges which can be utilized to reproduce the polarity of the solid material and the adsorbing molecules. Energy storage with hetero-clusters has described that the frame of the overcoming cluster is related to Pd–AlGaN or Pt–AlGaN in the high amounts of frequency. This property makes Pd–AlGaN or Pt–AlGaN potentially advantageous for certain high-frequency applications requiring transistor cells for energy storage due to hydrogen adsorption by formation of AlGaN–H, Si–AlGaN–H, Ge–AlGaN–H, Pd–AlGaN–H or Pt–AlGaN–H. The advantages of platinum or palladium over aluminum gallium nitride include its higher electron and hole mobility, allowing platinum or palladium doping devices to operate at higher frequencies than silicon or germanium doping devices. Thus, it should be explored its unique properties, such as its ability to increase energy storage which could lead to advancements transistors.

ACKNOWLEDGMENTS

In successfully completing this paper and its research, the authors are grateful to Kastamonu University.

FUNDING

This work was supported by ongoing institutional funding. No additional grants to carry out or direct this particular research were obtained.

CONFLICT OF INTEREST

The authors of this work declare that they have no conflicts of interest.

REFERENCES

1. S. K. Dolukhanyan, A. G. Aleksanyan, O. P. Ter-Galstyan, et al., Russ. J. Phys. Chem. B **16**, 76–83 (2022). https://doi.org/10.1134/S1990793122010043
2. F. Mollaamin and M. Monajjemi, Comput. Theor. Chem. **1237**, 114646 (2024). https://doi.org/10.1016/j.comptc.2024.114646
3. C. Li, X. Chen, and Z. Wang, Micromachines **15**, 330 (2024). https://doi.org/10.3390/mi15030330
4. Z. Wang, J. Comput. Electron. **18**, 1251–1258 (2019). https://doi.org/10.1007/s10825-019-01383-7
5. S. Mishra, P. Kachhawa, P. Mondal, et al., IEEE Trans. Electron. Devices **69**, 4527–4533 (2022). https://doi.org/10.1109/TED.2022.3184658
6. Z. Wang, J. Cao, F. Wang, et al., Superlattices Microstruct. **122**, 343–348 (2018). https://doi.org/10.1016/j.spmi.2018.07.016
7. A. M. Bhat, C. Periasamy, R. Poonia, et al., IEEE Trans. Nanotechnol. **22**, 466–472 (2023). https://doi.org/10.1109/TNANO.2023.3305360
8. Z. Wang, Z. Zhang, S. Wang, et al., Appl. Sci. **9**, 3054 (2019). https://doi.org/10.3390/app9153054
9. S. Yang, J. Yan, M. He, et al., Russ. J. Phys. Chem. A **93**, 2817–2823 (2019). https://doi.org/10.1134/S003602441913034X
10. R. Blasco, A. Ajay, E. Robin, et al., J. Phys. D: Appl. Phys. **52**, 125101(2019). https://doi.org/10.1088/1361-6463/aafec2
11. D. Wang, X. Liu, S. Fang, et al., Nano Lett. **21**, 120–129 (2021). https://doi.org/10.1021/acs.nanolett.0c03357
12. M. Monajjemi, F. Mollaamin, S. Shahriari, et al., Russ. J. Phys. Chem. B **18**, 1217–1225 (2024). https://doi.org/10.1134/S1990793124700349
13. A. Sun, H. Yu, Y. Zhou, et al., Int. J. Hydrogen Energy. **47**, 17494–17503 (2022). https://doi.org/10.1016/j.ijhydene.2022.03.185
14. F. Mollaamin and M. Monajjemi, Russ. J. Phys. Chem. B **18**, 1177–1198 (2024). https://doi.org/10.1134/S1990793124700507

15. Q. Q. Xiong, Russ. J. Phys. Chem. B **18**, 638–644 (2024). https://doi.org/10.1134/S1990793124700155
16. F. Mollaamin and M. Monajjemi, Russ. J. Phys. Chem. B **18**, 1199–1216 (2024). https://doi.org/10.1134/S1990793124700519
17. F. Mollaamin and M. Monajjemi, J. Carbon Res. **9**, 20 (2023).
18. S. Shahriari, M. Monajjemi, and F. Mollaamin, J. Chil. Chem. Soc. **67**, 5468–5476 (2022). https://doi.org/10.4067/S0717-97072022000205468
19. M. A. A. Zadeh, H. Lari, L. Kharghanian, et al., J. Comput. Theor. Nanosci. 12, 4358 (2015). https://doi.org/10.1166/jctn.2015.4366
20. F. Mollaamin and M. Monajjemi, Sensor Review 43, 266–279 (2023). https://doi.org/10.1108/SR-03-2023-0040
21. M. Monajjemi, H. Yamola, and F. Mollaamin, Fullerenes Nanotubes Carbon Nanostruct. **22**, 595–603 (2014). https://doi.org/10.1080/1536383X.2012.702163
22. F. Mollaamin, F. Najafi, M. Khaleghian, B. Khalili Hadad, and M. Monajjemi, Fullerenes Nanotubes Carbon Nanostruct. **19**, 653–667 (2011). https://doi.org/10.1080/1536383X.2010.504956
23. S. Shahriari, F. Mollaamin, and M. Monajjemi, Micromachines **14**, 241(2023). https://doi.org/10.3390/mi14020241
24. F. Mollaamin and M. Monajjemi, Clean Technol. **5**, 403–417 (2023). https://doi.org/10.3390/cleantechnol5010020
25. F Mollaamin and M. Monajjemi, J. Comput. Theor. Nanosci. **12**, 1030–1039 (2015). https://doi.org/10.1166/jctn.2015.3846
26. F Mollaamin and M. Monajjemi, J. Bio- Tribo-Corros. **9**, 33 (2023). https://doi.org/10.1007/s40735-023-00751-y
27. F. Mollaamin, M. Monajjemi, S. Salemi, et al., Fullerenes Nanotubes Carbon Nanostruct. **19**, 182 (2011). https://doi.org/10.1080/15363831003782932
28. M. Monajjemi, M. Khaleghian, N. Tadayonpour, et al., Int. J. Nanosci. **09**, 517–529 (2010). https://doi.org/10.1142/S0219581X10007071
29. F. Mollaamin and M. Monajjemi, J. Cluster Sci. **34**, 2901–2918 (2023). https://doi.org/10.1007/s10876-023-02436-5
30. F. Mollaamin and M. Monajjemi, J. Mol. Model. **29**, 119 (2023). https://doi.org/10.1007/s00894-023-05526-3
31. F. Mollaamin and M. Monajjemi, Russ. J. Phys. Chem. B **17**, 658–672 (2023). https://doi.org/10.1134/S1990793123030223
32. N. Pant, Z. Deng, E. Kioupakis, Appl. Phys. Lett. **117**, 242105 (2020). https://doi.org/10.1063/5.0027802
33. F. Mollaamin and Monajjemi, M. Russ. J. Phys. Chem. B **18**, 607–623 (2024). https://doi.org/10.1134/S1990793124020271
34. F. Mollaamin, S. Shahriari, and Monajjemi, M. Russ. J. Phys. Chem. B **18**, 398–418 (2024). https://doi.org/10.1134/S199079312402026X
35. F. Mollaamin, Russ. J. Phys. Chem. B **18**, 805–820 (2024). https://doi.org/10.1134/S1990793124700131
36. M. Monajjemi, F. Mollaamin, M. R. Gholami, et al., Main Group Metal Chemistry **26**, 349–361 (2003). https://doi.org/10.1515/MGMC.2003.26.6.349
37. M. Monajjemi, A. Sobhanmanesh, and F. Mollaamin, Fullerenes, Nanotubes and Carbon Nanostructures **21**, 47–63 (2013). https://doi.org/10.1080/1536383X.2011.574325
38. F. Mollaamin, Computation **11**, 84 (2023). https://doi.org/10.3390/computation11040084
39. F. Mollaamin, S. Mohammadi, Z. Khalaj, et al., Russ. J. Phys. Chem. B **18**, 67–82 (2024). https://doi.org/10.1134/S1990793124010330
40. A. M. Tereza, G. L. Agafonov, E. K. Anderzhanov, et al., Russ. J. Phys. Chem. B **18**, 965–972 (2024). https://doi.org/10.1134/S1990793124700416
41. A. A. Belyaev and B. S. Ermolaev, Russ. J. Phys. Chem. B **18**, 988–1001 (2024). https://doi.org/10.1134/S1990793124700532
42. E. A. Salgansky, M. V. Salganskaya, and I. V. Sedov, Russ. J. Phys. Chem. B **18**, 1042–1047 (2024). https://doi.org/10.1134/S1990793124700593
43. A. E. Smygalina and A. D. Kiverin, Russ. J. Phys. Chem. B **18**, 1048–1059 (2024). https://doi.org/10.1134/S199079312470060X
44. M. Monajjemi, F. Mollaamin, S. Shahriari, et al., Russ. J. Phys. Chem. B **18**, 1090–1112 (2024). https://doi.org/10.1134/S1990793124700465
45. F. Mollaamin and M. Monajjemi, Russ. J. Phys. Chem. B **18**, 533–548 (2024). https://doi.org/10.1134/S199079312402012X
46. B. Khalili Hadad, F. Mollaamin, and M. Monajjemi, Russ. Chem. Bull. **60**, 238–241 (2011). https://doi.org/10.1007/s11172-011-0039-5
47. F. Mollaamin, S. Mohammadi, Z. Khalaj, et al., Russ. J. Phys. Chem. B **18**, 67–82 (2024). https://doi.org/10.1134/S1990793124010330
48. M. Monajjemi, F. Mollaamin, and S. Shojaei, Biointerface Res. Appl. Chem. **10**, 5575 (2020). https://doi.org/10.33263/BRIAC103.575585
49. F. Mollaamin and M. Monajjemi, Comput. Theor. Chem. **1237**, 114666 (2024). https://doi.org/10.1016/j.comptc.2024.114666
50. S. Shahriari, F. Mollaamin, and M. Monajjemi, Micromachines **14**, 241 (2023). https://doi.org/10.3390/mi14020241
51. F. Mollaamin and M. Monajjemi, J. Mol. Struct. **1300**, 137214 (2024). https://doi.org/10.1016/j.molstruc.2023.137214
52. F. Mollaamin, A. Ilkhani, N. Sakhaei, et al., J. Comput. Theor. Nanosci. **12**, 3148–3154 (2015). https://doi.org/10.1166/jctn.2015.4092
53. F. Mollaamin and M. Monajjemi, Sens. Rev. **44**, 179–193 (2024). https://doi.org/10.1108/SR-01-2024-0066

54. M. Monajjemi, L. Mahdavian, F. Mollaamin, et al., Russ. J. Inorg. Chem. **54**, 1465–1473 (2009). https://doi.org/10.1134/S0036023609090216

55. F. Mollaamin and M. Monajjemi, Russ. J. Phys. Chem. B **18**, 49–66 (2024). https://doi.org/10.1134/S1990793124010159

56. F. Mollaamin and M. Monajjemi, Int. J. Quantum Chem. **124**, e27348 (2024). https://doi.org/10.1002/qua.27348

57. S. V. Feskov, Russ. J. Phys. Chem. B **18**, 1–8 (2024). https://doi.org/10.1134/S1990793124010081

58. F. Mollaamin and M. Monajjemi, Mol. Simul. **49**, 365–376 (2023). . https://doi.org/10.1080/08927022.2022.2159996

59. M. J. Frisch, G. W. Trucks, H. B. Schlegel, G. E. Scuseria, M. A. Robb, J. R. Cheeseman, G. Scalmani, V. Barone, G. A. Petersson, H. Nakatsuji, X. Li, M. Caricato, A. V. Marenich, J. Bloino, B. G. Janesko, R. Gomperts, B. Mennucci, H. P. Hratchian, J. V. Ortiz, A. F. Izmaylov, J. L. Sonnenberg, D. Williams-Young, F. Ding, F. Lipparini, F. Egidi, J. Goings, B. Peng, A. Petrone, T. Henderson, D. Ranasinghe, V. G. Zakrzewski, J. Gao, N. Rega, G. Zheng, W. Liang, M. Hada, M. Ehara, K. Toyota, R. Fukuda, J. Hasegawa, M. Ishida, T. Nakajima, Y. Honda, O. Kitao, H. Nakai, T. Vreven, K. Throssell, J. A. Montgomery, Jr., J. E. Peralta, F. Ogliaro, M. J. Bearpark, J. J. Heyd, E. N. Brothers, K. N. Kudin, V. N. Staroverov, T. A. Keith, R. Kobayashi, J. Normand, K. Raghavachari, A. P. Rendell, J. C. Burant, S. S. Iyengar, J. Tomasi, M. Cossi, J. M. Millam, M. Klene, C. Adamo, R. Cammi, J. W. Ochterski, R. L. Martin, K. Morokuma, O. Farkas, J. B. Foresman, and D. J. Fox, *Gaussian 16, Revision C.01* (Gaussian, Inc., Wallingford CT, 2016).

60. R. Dennington, T. A. Keith, and J. M. Millam, GaussView, *Version 6.06.16* (Semichem Inc., Shawnee Mission, KS, 2016).

61. T. Yanai, D. P. Tew, and N. C. Handy, Chem. Phys. Lett. **393**, 51–57 (2004). https://doi.org/10.1016/j.cplett.2004.06.011

62. S. Grimme, A. Hansen, J. G. Brandenburg, et al., Chem. Rev. **116**, 5105–5154 (2016). https://doi.org/10.1021/acs.chemrev.5b00533

63. A. D. Becke and K. E. Edgecombe, J. Chem. Phys. **9**, 5397–5403(1990). https://doi.org/10.1063/1.458517

64. S. N. Steinmann, Y. Mob, and C. Corminboeuf, Phys. Chem. Chem. Phys. **13**, 20584–20592 (2011). https://doi.org/10.1039/C1CP21055F

65. L. Tian, C. Feiwu, and W. Xuebao, Acta Phys. Chim. Sin. **27**, 2786–2792(2011). https://doi.org/10.3866/PKU.WHXB20112786

66. A. Savin, O. Jepsen, J. Flad, et al., Angew. Chem. Int. Edit. Engl. **31**, 187 (1992). https://doi.org/10.1002/anie.199201871

67. Z. Xu, C. Qin, Y. Yu, et al., AIP Adv. **14**, 055114 (2024). https://doi.org/10.1063/5.0208082

68. E. I. Rudenko, N. V. Dohlikova, A. K. Gatin, et al., Russ. J. Phys. Chem. B **17**, 845–852 (2023). https://doi.org/10.1134/S1990793123040164

69. D. A. Krugovov, A. K. Gatin, N. V. Potapova, et al., Russ. J. Phys. Chem. B **18**, 656–662 (2024). https://doi.org/10.1134/S199079312470012X

70. V. I. Petinov, V. M. Timin, K. V. Bozhenko, et al., Russ. J. Phys. Chem. B **18**, 365–368 (2024). https://doi.org/10.1134/S1990793124020301

71. A. M. Tereza, G. L. Agafonov, E. K. Anderzhanov, et al., Russ. J. Phys. Chem. B **17**, 1294–1299 (2023). https://doi.org/10.1134/S1990793123060246

72. D. Mayilyan and A. Aleksanyan, Russ. J. Phys. Chem. B **17**, 1177–1182 (2023). https://doi.org/10.1134/S199079312305007X

73. A. E. Smygalina and A. D. Kiverin, Russ. J. Phys. Chem. B **17**, 907–914 (2023). https://doi.org/10.1134/S1990793123040188

74. A. M. Tereza, G. L. Agafonov, E. K. Anderzhanov, et al., Russ. J. Phys. Chem. B **17**, 974–978 (2023). https://doi.org/10.1134/S1990793123040309

75. M. I. Ikim, E. Y. Spiridonova, V. F. Gromov, et al., Russ. J. Phys. Chem. B **17**, 774–777 (2023). https://doi.org/10.1134/S199079312303003X

76. A. H. Davtyan, Z. O. Manukyan, S. D. Arsentev, et al., Russ. J. Phys. Chem. B **17**, 336–345 (2023). https://doi.org/10.1134/S1990793123020239

77. S. I. Sumskoi, A. S. Sof'in, S. K. Zainetdinov, et al., Russ. J. Phys. Chem. B **17**, 419–424 (2023). https://doi.org/10.1134/S199079312302015X

78. K. Y. Troshin, N. M. Rubtsov, G. I. Tsvetkov, et al., Russ. J. Phys. Chem. B **17**, 433–438 (2023). https://doi.org/10.1134/S1990793123020185

79. F. Mollaamin, S. Shahriari, M. Monajjemi, et al., J. Cluster Sci. **34**, 1547–1562 (2023). https://doi.org/10.1007/s10876-022-02335-1

80. F. Mollaamin and M. Monajjemi, J. Mol. Model. **29**, 170 (2023). https://doi.org/10.1007/s00894-023-05567-8

81. F. Mollaamin, J. Comput. Theor. Nanosci. **11**, 2393–2398 (2014). https://doi.org/10.1166/jctn.2014.3653